Chemical Science

Accepted Manuscript

This article can be cited before page numbers have been issued, to do this please use: X. Li, J. Liu, Y. Zhang, Z. Dai, Z. Tan, H. Yang, C. Xu, M. Strømme, S. Zhou and Z. Li, *Chem. Sci.*, 2026, DOI: 10.1039/D6SC01290F.

ROYAL SOCIETY OF CHEMISTRY

rsc.li/chemical-science

View Article Online
DOI: 10.1039/D6SC01290F

Fast Hydrated-Ion Transport and Desolvation in Pyridinyl COF Membranes via Competitive Coordination

Xuan Li,[1] Jiaxin Liu, [1] Yilin Zhang,[1] Zhixiang Dai,[1] Zihan Tan,[1] Hongli Yang,[1] Chao Xu,[2] Maria Strømme,[2] Shengyang Zhou, [1,] Zhong-Ming Li[1]*

[1]College of Materials Science and Engineering, College of Polymer Science and Engineering, State Key Laboratory of Advanced Polymer Materials, Sichuan University, Chengdu 610065, China

[2]Department of Materials Science and Engineering, The Ångström Laboratory, Uppsala University, Uppsala 752 37, Sweden

[*]E-mail: shengyang.zhou@scu.edu.cn

View Article Online
DOI: 10.1039/D6SC01290F

Abstract

Hydrated-ion transport and desolvation dominate energy transfer and ionic selectivity in membrane separation, electrochemical energy storage, and catalytic systems, whereas achieving fast ion conduction with low hydration remains highly challenging. In this work, we discover that pyridinyl-based covalent organic frameworks (COFs) membranes enable the fast transport of hydrated-ions with efficient desolvation. This originates from a soft Lewis acid-mediated competitive coordination mechanism, where pyridinyl groups partially displace hydration shells. The ordered channels with optimized coordination not only stabilize desolvated ions but also provide continuous hopping pathways for ion migration, resulting in rapid ion transport with reduced desolvation barriers. As a proof-of-concept application, the pyridinyl COFs membranes were studied in aqueous zinc batteries. Electrochemical tests reveal that partial zinc ions desolvation lowers the thermodynamic barrier for zinc nucleation, while rapid ion transport balances interfacial reaction kinetics, effectively suppressing dendrite growth and parasitic reactions. Consequently, zinc anode paired with pyridyl COFs membranes exhibits reversible stripping/plating over 2000 cycles in a conventional $ZnSO_4$ electrolyte without additives, outperforming most of the current aqueous battery separators. This work demonstrates the unique desolvation transport behavior of hydrated-ions in pyridinyl COFs membranes and provides new insights for the rational design of COFs for electrochemical energy storage.

View Article Online
DOI: 10.1039/D6SC01290F

Introduction

The regulation of hydrated ions is fundamental to a wide range of energy storage,[1, 2] chemical separation engineering,[3, 4] and catalytic systems[5, 6] since ion transport and desolvation directly control energy transfer, ionic selectivity, and reaction kinetics.[7, 8] In membrane systems, precise control of ion coordination environments and migration pathways determines the efficiency and specificity of ion transport and its overall performance.[9-11] This modulation becomes particularly critical in electrochemical energy storage devices such as aqueous batteries, where hydrated ions must traverse both the electrolyte and electrode interfaces, and their solvation structures directly influence the thermodynamics and kinetics of electrochemical reactions.[12, 13] For example, Zn^{2+} in aqueous zinc-ion batteries exists in fully hydrated states, and the energy required to partially remove water molecules from their hydration shell directly affects nucleation overpotential, deposition uniformity, and the likelihood of dendrite formation.[14-17] Rapid ion conduction under low hydration conditions is therefore essential to maintain uniform ion flux, enhance charge transfer, and suppress parasitic reactions at the electrode-electrolyte interface. Achieving both low solvation and high mobility is particularly challenging because de-hydration processes are energetically demanding. Conventional membranes rarely provide the chemical functionality and well-defined pore topology necessary to facilitate ion desolvation and stabilize partially desolvated ions. They also lack the ordered architecture required to guide the directional transport of partially desolvated ions and to reduce the thermodynamic barriers associated with their low-solvation state and limited stability.[18, 19] Consequently, the

View Article Online
DOI: 10.1039/D6SC01290F

rational design of materials capable of efficient low-hydrated ion transport remains a major scientific and engineering challenge with broad implications for improving the efficiency, stability, and safety of electrochemical energy storage devices, as well as for advancing catalysis, selective ion separations, and other processes dependent on controlled ion transport.

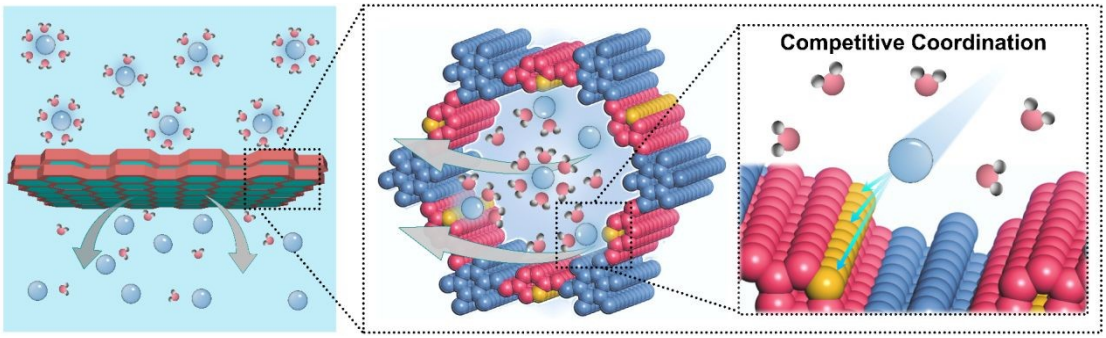

Schematic 1. Schematic illustration of pyridinyl COFs membrane for rapid transport and partial desolvation of hydrated ions via a competitive coordination mechanism.

In this work, we find that pyridinyl-functionalized covalent organic framework (COFs) membranes can realize the rapid transmembrane transport of hydrated ions while facilitating their partial desolvation. This behavior arises from a soft Lewis acid-mediated competitive coordination mechanism in which pyridinyl groups selectively interact with hydrated ions and partially displace water molecules from their hydration shells (Schematic 1). Such regulated desolvation is cooperatively supported by the spatial confinement and structural ordering of the COFs nanochannels, which stabilize partially desolvated ions and reduce the energetic barrier associated with low solvation transport, thereby enabling directional and efficient ion conduction. To elucidate the roles of pyridinyl coordination and pore topology in this process, two structurally related COFs membranes containing single pyridine and bipyridine units were designed

View Article Online
DOI: 10.1039/D6SC01290F

and fabricated. Comparative analysis reveals that the single pyridine COFs membrane establishes a moderate competitive coordination environment within confined nanochannels. This environment enables effective ion desolvation, accelerates diffusion, and preserves thermodynamic stability. In contrast, the bipyridine COFs exhibits excessive coordination that leads to ion immobilization and slowed migration, thereby lowering desolvation efficiency. As a conceptual validation of this transmembrane ion regulation strategy, both COFs membranes were evaluated in aqueous zinc battery (AZB) systems. Electrochemical results demonstrate that regulated zinc ion desolvation and transport within confined nanochannels lower the thermodynamic barrier for Zn nucleation and balance the kinetic rates of ion diffusion and surface deposition. This synergy ensures uniform ion flux, promotes homogeneous zinc growth, and effectively suppresses dendrite formation and parasitic reactions such as hydrogen evolution and local hydroxide accumulation. Consequently, zinc anodes paired with the single pyridine COFs membrane exhibit stable stripping and plating over 2000 cycles (>5000 hours) in a conventional 2 M $ZnSO_4$ electrolyte without additives, obviously outperforming most currently used separators in AZBs. These results exhibit that the rational design of chemical sites combined with the highly ordered nanochannel architecture of COFs membranes provides an effective platform to couple ion solvation thermodynamics with transport kinetics. They also highlight the potential of COFs for the development of next-generation ion-regulating membranes and offer theoretical inspiration for their broader applications in electrochemical energy storage, separation technology, catalysis engineering, and membrane-based ion

View Article Online
DOI: 10.1039/D6SC01290F

regulation.

Results and Discussion

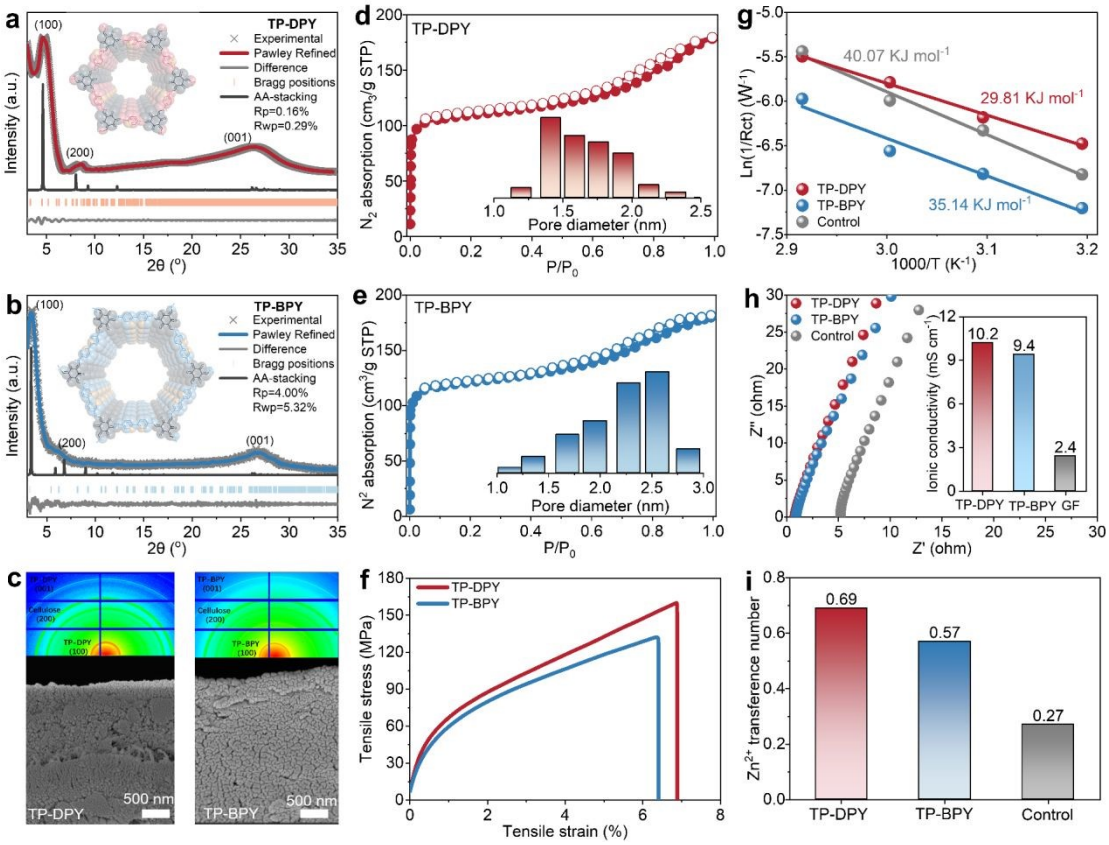

Figure 1. Structural characterization and hydrated ion transport properties of two pyridine COFs membranes. Experimental and simulated XRD patterns with corresponding molecular models of (a) TP-DPY and (b) TP-BPY COFs. (c-d) N_2 sorption isotherms and calculated pore size distributions, (e) SEM images and corresponding 2D-WAXS patterns, (f) mechanical tensile stress-strain curves of two COFs membranes. (g) *Arrhenius* activation energy, (h) *Nyquist* plots and calculated ionic conductivity, (i) zinc ion transference numbers of two COFs membranes and bulk $ZnSO_4$ electrolyte as control, respectively.

Two pyridine-based COFs, TP-DPY and TP-BPY, were synthesized via a one-step condensation reaction of 2,4,6-triformylphloroglucinol (TP) with 2,6-diaminopyridine (DPY) or 2,2′-bipyridine-5,5′-diamine (BPY), as illustrated in Figure S1 and Figure S2.[20, 21] An aqueous synthesis route was employed using water as the solvent and acetic acid as the catalyst, representing an environmentally-friendly approach to conventional

View Article Online
DOI: 10.1039/D6SC01290F

solvothermal methods that rely on organic solvents. This method allowed the formation of highly crystalline COFs under ambient temperature and pressure, as confirmed by X-ray diffraction patterns in Figure 1a and Figure 1b. Both COFs are constructed through *β*-ketoenamine linkages, which impart robust chemical stability and hydrolytic resistance, making them suitable for prolonged operation in aqueous environments.[20, 21] The formation of the two pyridyl-based COFs was further confirmed by multiple spectroscopic techniques. Solid-state ^{13}C nuclear magnetic resonance (^{13}C NMR) and Fourier-transform infrared (FTIR) spectroscopy show the characteristic signals of C=O, C–N, consistent with the typical chemical structure of the *β*-ketoenamine linked COFs (Figure S3 and Figure S4). For membrane fabrication, nanocellulose was incorporated as a binder, and a vacuum-assisted filtration technique was applied (Figure S5).[22] This straightforward procedure yielded freestanding and flexible membranes from COFs powders with uniform thickness (Figure S6). Scanning electron microscopy (SEM) images reveal dense and homogeneously packed COFs particles within both membranes, while two-dimensional wide-angle X-ray scattering (2D-WAXS) and energy dispersive spectroscopy (EDS) analyses confirm an isotropic distribution of COFs crystals, highlighting the uniformity of the membrane microstructure (Figure 1c, Figure S6-S8). Nitrogen adsorption analysis indicates a highly porous structure of those two COFs membranes dominated by micropores of 1-2 nm, arising from the intrinsic nanopores of the COFs skeleton (Figure 1d-e). Mechanical characterization demonstrated that both COFs membranes exhibit tensile strengths over 100 MPa (Figure 1f), which are substantially higher than those of COFs membranes prepared via

View Article Online
DOI: 10.1039/D6SC01290F

conventional two-phase interfacial methods that typically show tensile strengths below 5 MPa. The combination of highly ordered, uniform nanochannels and robust mechanical integrity renders these two COFs membranes an ideal and stable platform for electrochemical investigations, providing well-defined confined pathways for ion transport under practical operating conditions.

Water contact angle measurements reveal that both pyridine-based COF membranes exhibit initially contact angles of approximately 40-50°. After ten minutes of contact, the angles decrease to below 20°, confirming their obvious hydrophilic nature (Figure S9). This wetting behavior is essential for ensuring uniform and stable electrolyte infiltration for reliable operation in aqueous environments. The zinc ion transport properties of the two COFs membranes were systematically evaluated in comparison with the bulk 2 M $ZnSO_4$ electrolyte as a control. As shown in Figure 1g, the Arrhenius activation energy is substantially lower for the TP-DPY and TP-BPY membranes than for the bulk electrolyte, decreasing from 40.07 kJ mol^{-1} to 29.81 kJ mol^{-1} and 35.14 kJ mol^{-1}, respectively (Figure S10-S11, Table S2). This decrease in activation energy reflects accelerated Zn^{2+} migration within the ordered COFs channels and indicates improved ion transport kinetics compared with the bulk electrolyte. As a result, both COFs membranes exhibit zinc ion conductivities approaching up to ~10 mS cm^{-1}, which is for time higher than that of the bulk electrolyte with 2.4 mS cm^{-1} (Figure 1h). COF Membrane thickness has little effect on the Zn^{2+} ionic conductivity of the COF membranes (Figure S12). In addition, the zinc ion transference numbers also show remarkable improvement, reaching 0.69 and 0.57 for both TP-DPY and TP-BPY

View Article Online
DOI: 10.1039/D6SC01290F

membranes, respectively, compared with 0.27 for the bulk electrolyte (Figure 1i and Figure S13). The reduced Arrhenius activation energy, together with the enhanced Zn^{2+} conductivity and transference number, demonstrates that the COFs membranes establish cation-selective, low-barrier transport pathways, thereby accelerating Zn^{2+} transport kinetics. This behavior confirms that Zn^{2+} serves as the dominant charge carrier, with more efficient and selective ion conduction within the COFs membranes.

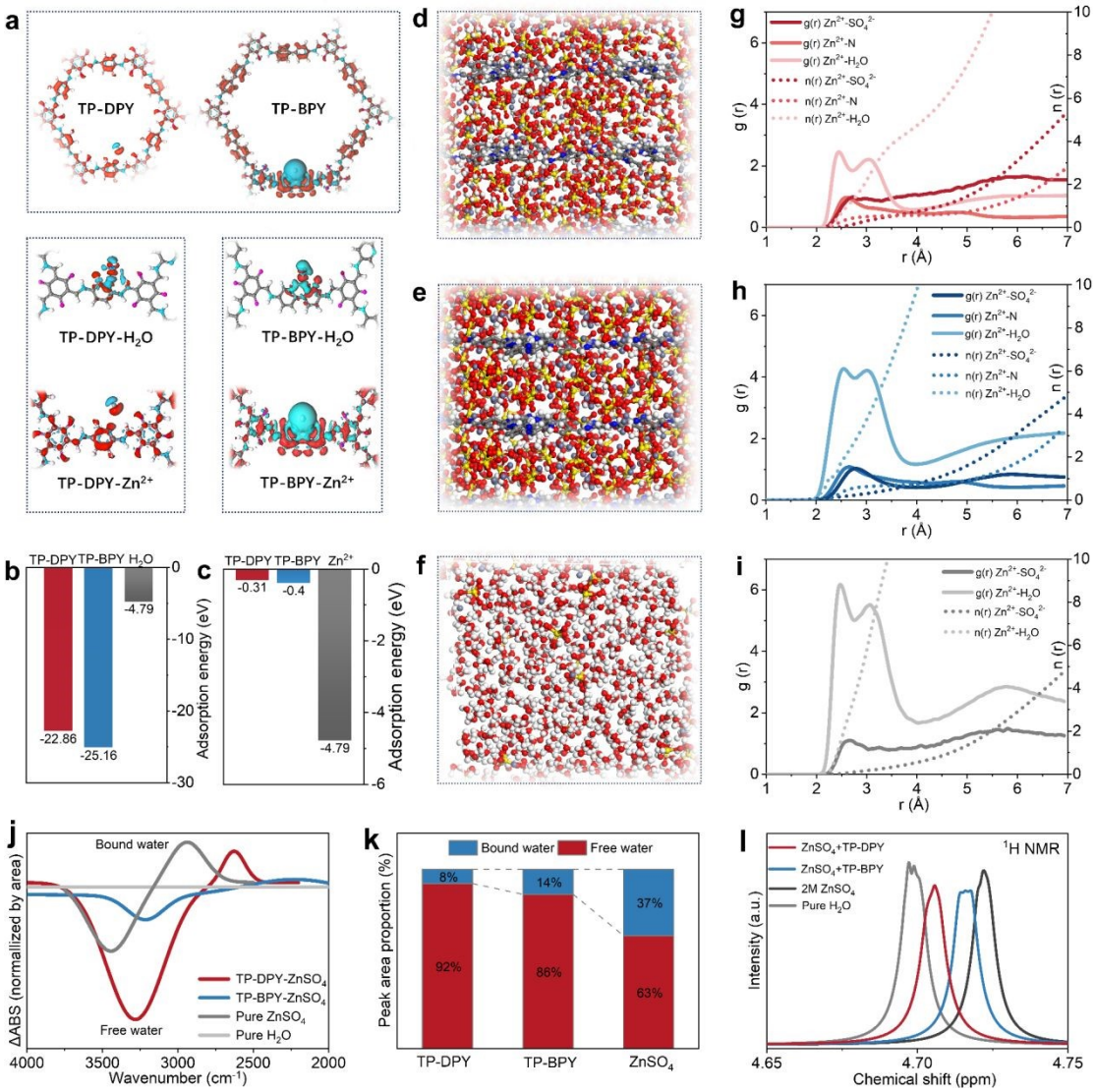

Figure 2. Mechanistic insights into hydrated ion transport behaviors in pyridinyl COFs membranes. (a) Charge density difference profiles and corresponding enlarged views of TP-DPY and TP-BPY calculated by density functional theory (DFT). Calculated interaction energies of (b) Zn^{2+} and (c) H_2O with different molecular structures. Molecular dynamics (MD) simulation snapshots of $ZnSO_4$ electrolyte within (d) TP-DPY, (e) TP-BPY, and (f) in bulk

solution. Simulated radial distribution functions (RDFs) and coordination numbers (CN) of Zn^{2+} in (g) TP-DPY, (h) TP-BPY, and (i) bulk $ZnSO_4$ electrolyte. (j) FTIR and (l) ^1H NMR spectra of pure water and 2M $ZnSO_4$ electrolytes with in different membranes. (k) The corresponding proportions of hydrogen bonds calculated based on FTIR spectra.

To investigate the origin of the low migration energy barrier and the unusual transport behavior of hydrated ions within the COFs membranes, density functional theory (DFT) calculations were conducted to systematically decouple and quantify the interactions of two pyridinyl COFs with zinc ions and water molecules.[23-26] We first calculated the charge density difference by subtracting the sum of the charge densities of the isolated COFs and Zn^{2+} from that of the combined COFs-Zn^{2+} system, thereby revealing the redistribution of electrons during their interaction. The results show that bipyridyl exhibits stronger electron donation and more pronounced charge polarization compared to mono-pyridyl, as shown in Figure 2a. The calculated adsorption energies suggest that pyridyl COFs bind Zn^{2+} significantly more strongly than Zn^{2+} interacts with water in bulk electrolyte (Figure 2b-c). It indicates that strong interactions with pyridinyl groups can thermodynamically remodel the local coordination environment of hydrated Zn^{2+} ions during their transport through the COFs channels. Meanwhile, we found that the adsorption energy of Zn^{2+} on the mono-pyridyl COFs (22.86 eV) is lower than that on the bipyridyl COFs (25.16 eV), indicating that binding strength is not positively correlated with ion conduction capability. This behavior actually aligns with the hopping mechanism in ion conduction, in which the moderate Zn^{2+} coordination in mono-pyridyl COFs promotes dynamic hopping by enabling fast coordination exchange along the channels, in agreement with the experimentally

View Article Online
DOI: 10.1039/D6SC01290F

observed reduction in Arrhenius activation energy and increase in the Zn^{2+} transference number in mono-pyridyl COFs membrane.

Based on the above results, we further conducted molecular dynamics (MD) simulations to investigate the fine coordination environment and dynamic interactions of hydrated Zn^{2+} ions confined within the nanochannels of TP-DPY and TP-BPY COFs membranes.[27-29] To better model the state of hydrated ions within COFs membranes, multilayer COFs crystal models were constructed. A 2 M $ZnSO_4$ aqueous solution was then introduced into the nanopores of the two pyridinyl COFs membranes (Figure 2d-f, Figure S14-16). Periodic boundary conditions were applied in all three dimensions, and simulations were performed at 298 K and 1 atm to allow equilibration of the solvation structures. The force fields for the COFs and ions were refined via DFT-based charge fitting to accurately capture interactions between Zn^{2+} and the chemical groups. Simulation results reveal that zinc ions migrate significantly faster in TP-DPY COFs membranes compared to TP-BPY COFs membranes. Meanwhile, the average coordination number of Zn^{2+} in TP-DPY COFs membranes is obviously lower than that in TP-BPY COFs membranes and bulk electrolyte (Figure 2g-i), reflecting a more labile and dynamically fluctuating hydration environment. It can be explained within the framework of hopping-based ion conduction because the moderate binding strength of mono-pyridyl groups facilitates rapid coordination and de-coordination events, which allow hydrated zinc ions to efficiently hop between pyridinyl sites. The high mobility naturally leads to a lower statistical average coordination number, as zinc ions do not remain fully coordinated at any single site for extended periods. In contrast, stronger

View Article Online
DOI: 10.1039/D6SC01290F

bipyridyl interactions in TP-BPY COFs kinetically trap zinc ions, rigidify the local solvation structure, reduce hopping frequency, and slow overall ion transport.

The desolvation behavior in pyridine-based COFs membranes was further experimentally confirmed by probing the state of water molecules using FTIR spectroscopy (Figure 2j-k, Figure S17 and Figure S18) and NMR spectroscopy (Figure 2l). Using ultrapure water as the reference, infrared difference spectroscopy was applied to the O-H stretching region from 4000 to 2000 cm^{-1} to quantitatively compare the relative fractions of free and bound water in bulk $ZnSO_4$ electrolyte and within two pyridinyl COFs membranes, as shown in Figure 2j, with the calculated results summarized in Figure 2k. In bulk $ZnSO_4$ electrolyte, approximately 37% of water exists in a coordinated bound state, whereas the fraction of bound water decreases markedly to 14% in TP-BPY and further to 8% in TP-DPY. This reduction indicates that confinement within pyridinyl COFs channels effectively weakens Zn^{2+}-water coordination and promotes partial disruption of the hydration structure. To further probe the state of water molecules in different environments, ^1H NMR spectrum was employed, as shown in Figure 2l. In bulk electrolyte, coordination of water to Zn^{2+} leads to a pronounced downfield shift to higher ppm values due to proton de-shielding induced by strong electrostatic interactions with the cation. In contrast, when hydrated Zn^{2+} ions are confined within pyridinyl COFs membranes, the water proton signals shift up-field toward lower ppm values that are closer to those of pure water, reflecting weakened Zn^{2+}-water interactions and a more labile solvation environment arising from competitive coordination with pyridinyl groups. These spectroscopic results provide

View Article Online
DOI: 10.1039/D6SC01290F

direct experimental evidence that pyridinyl COFs membranes can induce partial desolvation of Zn^{2+} ions, thereby decreasing the energetic barrier associated with ion transport. The more pronounced reduction of bound water in TP-DPY further highlights the advantage of mono-pyridyl units within membranes, whose moderate coordination strength facilitates efficient Zn^{2+} migration by balancing desolvation and dynamic hopping within the COFs channels.

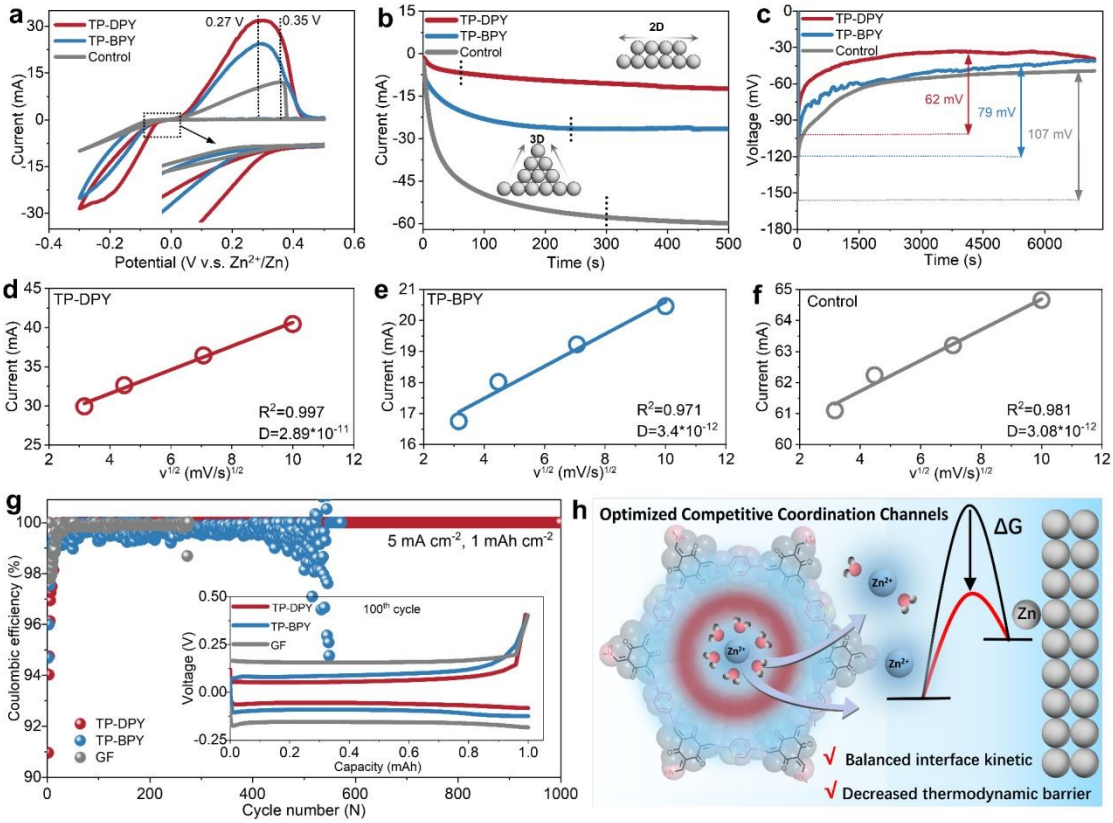

Figure 3. Electrochemical interfacial behavior of Zn electrode in aqueous electrolyte regulated by pyridine COFs membranes. (a) CV curves, (b) CA curves at a bias potential of -150 mV, and (c) CP curves at a current density of 1 mA cm^{-2}. Peak current vs. square root of scan rate plots for Zn||Cu cells paired with (d) TP-DPY membrane, (e) TP-BPY membrane, and (f) bulk electrolyte. (g) Coulombic efficiency of Zn||Cu cells at a current density of 5 mA cm^{-2}, the inset shows the 100^{th} charge-discharge profiles of Zn||Cu cells with two COFs membranes and bulk electrolyte. (h) Schematic of pyridinyl COFs membranes promoting simultaneous zinc ion transport and desolvation with reduced nucleation barriers and balanced interfacial kinetics on zinc anode.

The electrochemical interfacial behavior of Zn metal electrodes regulated by

View Article Online
DOI: 10.1039/D6SC01290F

pyridine COFs membranes was systematically investigated across various electrochemical devices, with glass fiber (GF) separators as the control group. Cyclic voltammetry (CV) analysis within Zn||Cu asymmetric cells demonstrates that TP-DPY and TP-BPY membranes yield lower stripping peak potentials, enhanced peak current densities, and more positive plating potentials relative to the control sample (Figure 3a). This behavior indicates reduced polarization and lower kinetic overpotentials for zinc stripping and plating, reflecting more efficient interfacial charge transfer and enhanced reaction reversibility enabled by the COFs membranes. Comparison between the two COFs membranes reveals that the TP-DPY-paired electrode exhibits higher stripping/plating currents, implying faster interfacial kinetics and more efficient zinc redox processes under identical polarization conditions. In chronoamperometry (CA) measurements, as shown in Figure 3b and Figure S20, cells assembled with COFs membranes display smaller and more stable current responses than the control counterpart, indicating a reduced instantaneous reaction rate and a more regulated ion reduction process at the electrode interface. This behavior reflects suppressed current fluctuations and mitigated concentration polarization of the zinc electrode by COFs membranes, suggesting that the deposition process proceeds through controlled nucleation and steady growth rather than rapid, unstable interfacial reactions. Simultaneously, chronopotentiometry (CP) measurements reveal that the zinc electrode assembled with pyridinyl COFs membranes exhibits a significantly lower nucleation overpotential and a more stable voltage plateau, indicating a reduced thermodynamic barrier for nucleation and facilitated uniform zinc deposition (Figure 3c).

View Article Online
DOI: 10.1039/D6SC01290F

To further investigate ion diffusion kinetics at the electrode surface mediated by two different COFs membranes, we measured the Zn^{2+} diffusion coefficients (D) in Zn-Cu cells assembled with the membranes (Figure 3d-f, Figure S21).[30] The TP-DPY-assembled cell exhibited a markedly higher diffusion coefficient (2.89×10^{-11} cm^2 s^{-1}) than the TP-BPY membrane (3.4×10^{-12} cm^2 s^{-1}) and the control cell (3.08×10^{-12} cm^2 s^{-1}). This result indicates that the mono-pyridinyl COFs membrane can substantially enhance interfacial ion mobility. The partial desolvation of Zn^{2+} induced by the COFs membranes reduces the reorganization energy for electron transfer, thereby lowering the kinetic barrier for reduction. At the same time, the combination of efficient ion transport and regulated local hydration level at the interface reshapes the free energy landscape for nucleation, decreasing the thermodynamic barrier for metal deposition. These features demonstrate that the COFs membranes, particularly TP-DPY, govern both the kinetic and thermodynamic aspects of zinc electrodeposition, enabling faster, energetically favorable, and controlled electrochemical deposition at the electrode surface. As a result, the TP-DPY-based cell maintained nearly 100% Coulombic efficiency over 1000 cycles of stripping/plating on Cu substrate, whereas the TP-BPY-based cell exhibited significant Coulombic efficiency fluctuations after 500 cycles, reflecting pronounced parasitic reactions and unstable zinc deposition, and short-circuited shortly thereafter (Figure 3g). In comparison, the control cell failed within 300 cycles. We collected XRD patterns of zinc deposited on the copper substrate after cycling test (Figure S22). Compared with the control sample, which exhibits clear diffraction peaks corresponding to side products $Zn_4SO_4(OH)_6 \cdot xH_2O$, no such peaks

View Article Online
DOI: 10.1039/D6SC01290F

were observed on Cu electrode paired with two COF membranes. This indicates that the COF membranes can effectively suppress the parasitic reaction and the formation of zinc surface byproducts and benefit a more uniform and stable metallic zinc deposition. Through a series of the above electrochemical and structural characterizations, it can be confirmed that pyridinyl COF membranes, particularly TP-DPY, enhance interfacial Zn^{2+} transport, effectively balancing surface diffusion and reaction kinetics at the electrode (Figure 3h). Simultaneously, COF-mediated partial desolvation lowers the reorganization energy and nucleation free energy, reducing thermodynamic barriers. This dual optimization of kinetics and thermodynamics enhances interfacial reactivity while suppressing parasitic side reactions. The combination of rapid ion conduction with reduced hydration ensures a controlled and stable deposition process, ultimately resulting in uniform, energetically favorable, and highly reversible electrochemical stripping/plating over extended cycling.[31-33]

View Article Online
DOI: 10.1039/D6SC01290F

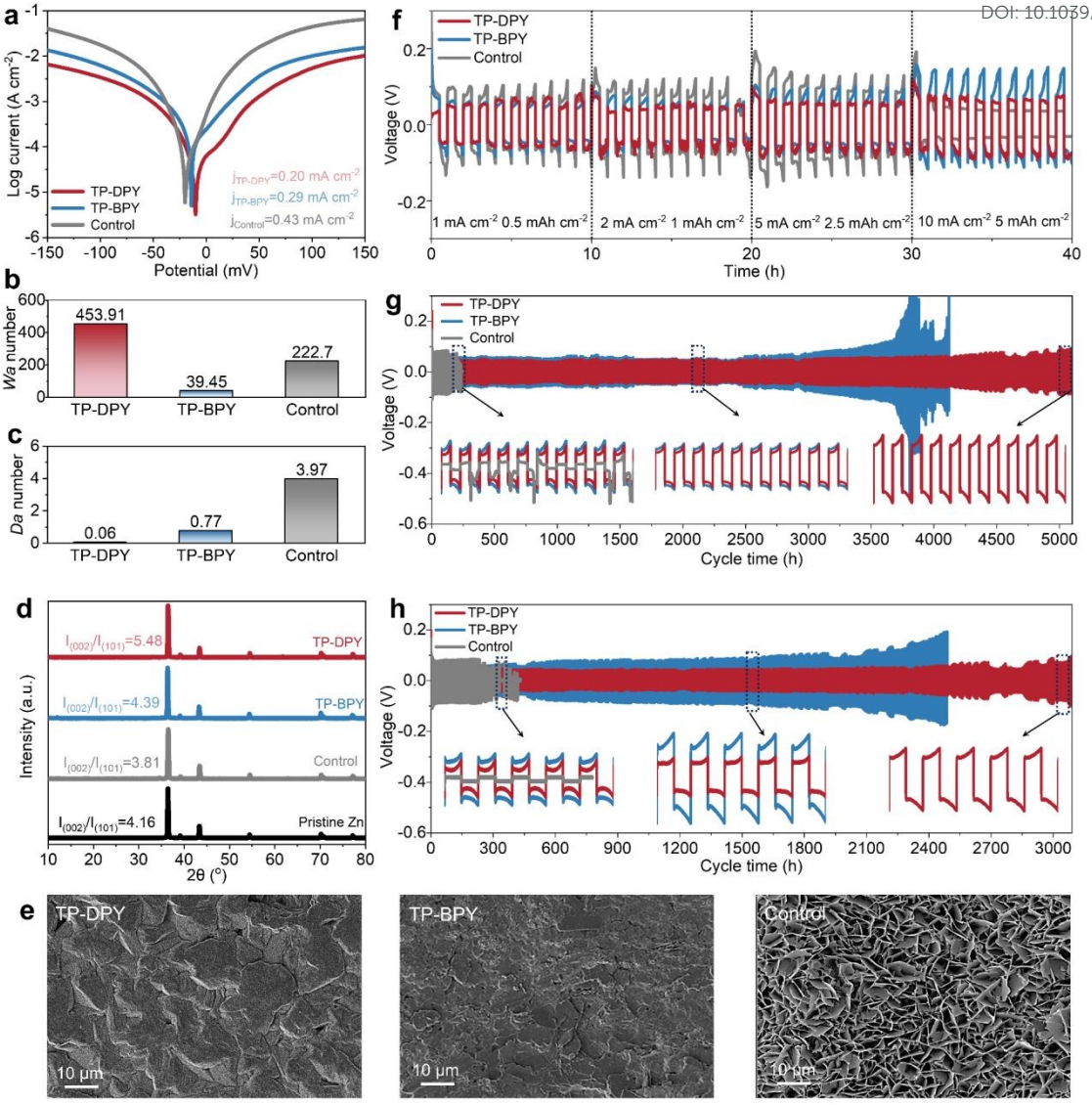

Figure 4. Electrochemical stability of Zn electrode in aqueous electrolyte regulated by pyridine COFs membranes. (a) *Tafel* plots, (b) W_a numbers, and (c) D_a numbers of Zn||Zn cells with different membranes. (d) XRD patterns and (e) SEM images of Zn electrode after 100 cycles. (f) Rate performance of Zn||Zn cells with different separators. Charge-discharge profiles of Zn||Zn symmetric cells with different membranes at a current density of (g) 1 mA cm^{-2} with an areal capacity of 1 mAh cm^{-2} and (h) 5 mA cm^{-2} with an areal capacity of 5 mAh cm^{-2}.

We systematically evaluated the electrochemical stability of zinc electrodes in aqueous electrolytes under the regulation of the two pyridinyl COF membranes. First, the Tafel curves of Zn||Zn symmetric cells paired with different membranes were collected to reveal the electrochemical corrosion behavior and deposition stability of

View Article Online
DOI: 10.1039/D6SC01290F

the zinc electrode in $ZnSO_4$ aqueous electrolyte. As shown in Figure 4a, the Tafel plots of cells assembled with TP-DPY, TP-BPY, and conventional GF separators as the control sample show that the corrosion current density is significantly reduced with both pyridine-based COFs separators. Specifically, cells assembled with TP-DPY and TP-BPY separators exhibit markedly reduced corrosion currents down to 0.20 and 0.29 mA cm^{-2}, respectively, compared to 0.43 mA cm^{-2} for the GF-assembled cell. Moreover, the TP-DPY-based cell shows a more negative corrosion potential. This indicates that pyridinyl COFs membranes effectively suppress zinc electrode corrosion by slowing spontaneous dissolution and enhancing interfacial stability. The more negative corrosion potential further reflects increased thermodynamic resistance to anodic dissolution. Together, these results demonstrate that the COFs membranes not only improve interfacial charge-transfer kinetics but also provide a more uniform and controlled Zn^{2+} deposition environment, thereby collectively enhancing the long-term stability of the electrode.

We further utilized the Damköhler (D_a) number and Wagner (W_a) number to investigate the impact of pyridine-based COF membranes on zinc deposition and dendrite growth behavior, which is crucial for the cycling stability of zinc electrodes. The D_a and W_a numbers evaluate the competition between diffusion and electrochemical reaction rates, respectively.[34-36] As shown in Figure 4b and Figure 4c, the cell assembled with the TP-DPY COFs membrane exhibits a larger W_a number and a smaller D_a number compared to the TP-BPY and control cells. This combination indicates that zinc deposition paired with the TP-DPY COFs membrane is primarily

View Article Online
DOI: 10.1039/D6SC01290F

diffusion-controlled rather than reaction-controlled. From a kinetic perspective, the deposition process is limited by Zn^{2+} diffusion rather than electron-transfer kinetics, suggesting that ion migration is governed by diffusion rates. From a thermodynamic perspective, TP-DPY COFs membrane minimizes the local supersaturation during nucleation. This effect can theoretically induce the uniform and dense zinc deposition. It can be confirmed by X-ray diffraction (XRD) and scanning electron microscopy (SEM) characterization. XRD patterns show that the pyridine-based COFs membrane does not significantly change the crystallographic orientation of the zinc crystal (Figure 4d). SEM images clearly show that the TP-DPY COFs membrane leads to more uniform and denser and smooth zinc deposition compared to that of the control electrode and with TP-BPY COFs membranes (Figure 4e and Figure S25). In addition, X-ray photoelectron spectroscopy (XPS) characterization was performed on zinc electrodes from Zn||Zn symmetric cells assembled with different membranes after long-term cycling to investigate the Zn chemical states on their surfaces (Figure S24). The results show that electrodes in cells with the TP-DPY COF membrane consist predominantly of metallic Zn, those with the TP-BPY membrane exhibit a minor divalent Zn (Zn^{2+}) signal, and those with the GF separator display a significant Zn^{2+} signal. Based on these observations, the formation of insoluble zinc byproducts can be inferred, indicating that COF membranes, particularly TP-DPY, effectively suppress parasitic reactions during cycling.

The cycling stability of zinc electrodes regulated by COF membranes was further evaluated using Zn||Zn symmetric cells. Rate performance tests indicate that with

View Article Online
DOI: 10.1039/D6SC01290F

increasing current density, cells assembled with the TP-BPY COFs membrane and the GF separator exhibit pronounced polarization. At a high current density of 10 mA cm^{-2}, cells with the GF separator even experience short-circuit failure (Figure 4f). In contrast, cells incorporating the TP-DPY COFs membrane maintain stable voltage profiles across all tested current densities without any signs of short-circuiting. During long-term cycling at a standard 1 mA cm^{-2} with an aerial capacity of 1 mAh cm^{-2}, the TP-DPY-paired cell operates stably for up to 5000 hours, far exceeding the lifespan of cells with GF (<300 hours) and TP-BPY (~4000 hours) membrane (Figure 4g). Even at an increased current density of 5 mA cm^{-2}, the TP-DPY-assembled cell continues to cycle steadily for up to 3000 hours (Figure 4h), demonstrating significantly improved cycling stability compared to that of GF and TP-BPY membranes. In fact, the membrane developed in this work, particularly the TP-DPY membrane, enables zinc electrodes to achieve cycling lifetimes that surpass those of most previously reported porous membranes used in AZBs (Table S4), highlighting the superior performance of competitive coordination design. In addition, we evaluated the deep stripping/plating performance of Zn||Zn symmetric cells assembled with different membranes, which is a stringent test of the stability of electrode with the ability to suppress parasitic reactions and dendrite growth. Under a high depth-of-discharge condition (DOD = 50%), the TP-DPY-based cell maintained stable cycling throughout the entire testing period (Figure S26). In contrast, the TP-BPY-based cell failed within fewer than ten cycles, while the cell using the GF separator showed no stable deep stripping and plating process. These results clearly demonstrate that the rapid hydrated zinc ion conduction and partial

View Article Online
DOI: 10.1039/D6SC01290F

desolvation facilitated by pyridinyl COFs membranes can substantially enhance the electrochemical cycling stability of zinc metal electrodes in aqueous electrolytes.

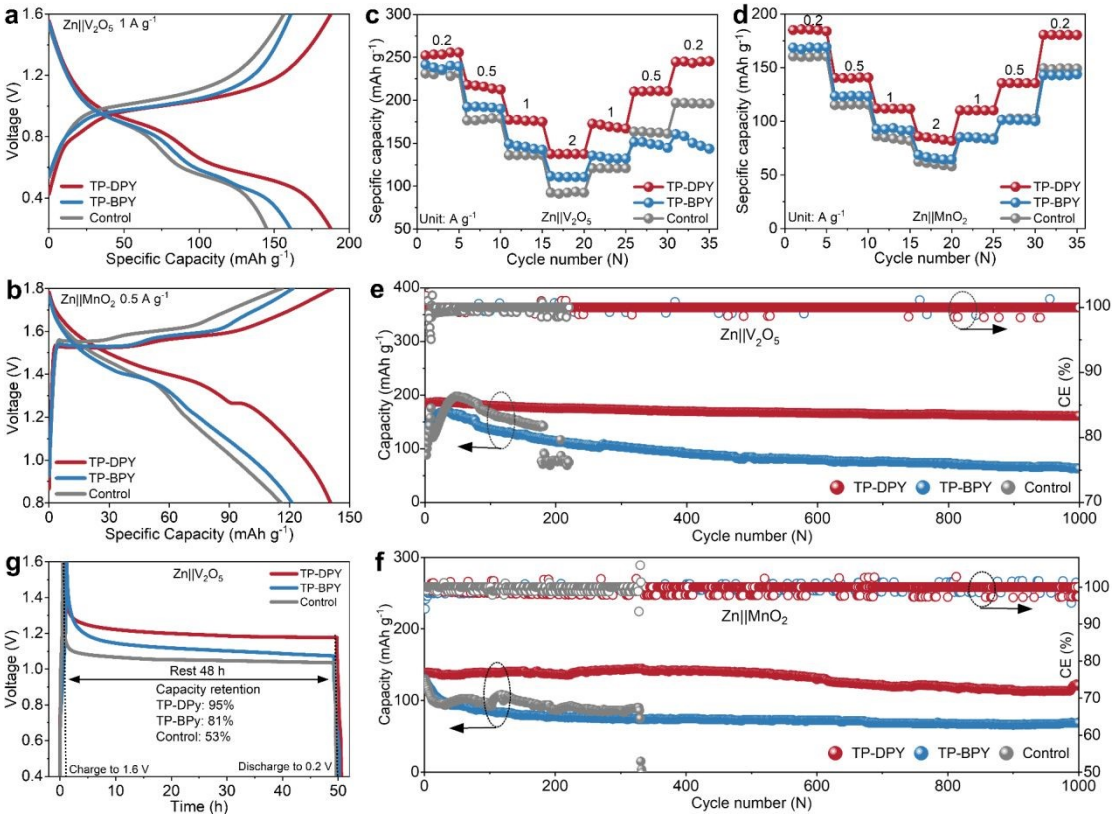

Figure 5. Electrochemical performance evaluation of pyridine COFs membranes in full battery systems. (a-b) Charge-discharge curves and (c) rate performance of Zn||MnO_2 and Zn||V_2O_5 full batteries paired with different membranes. (e) Discharge capacity and Coulombic efficiency of long-term cycling of Zn||V_2O_5 full batteries at 1 A g^{-1} and (f) Zn||MnO_2 full batteries at 0.5 A g^{-1}. (g) Self-discharge profiles of Zn||V_2O_5 full batteries with different membranes.

The electrochemical performance of two pyridine COFs membranes was further evaluated in full batteries by using commercial V_2O_5 and MnO_2 as cathode materials, respectively. In parallel, batteries paired with the conventional GF separator were also examined as control samples for comparative analysis. As is well known, V_2O_5 and MnO_2 store energy in aqueous zinc-ion batteries through reversible Zn^{2+} insertion and extraction accompanied by reversible redox transitions of the metal centers, [37]which places stringent requirements on electrolyte ions to exhibit high mobility and a reduced

View Article Online
DOI: 10.1039/D6SC01290F

solvation shell so as to support rapid diffusion, suppress polarization, and maintain the structural stability of the cathode. Figure 5a and Figure 5b present the charge-discharge profiles of Zn||V_2O_5 and Zn||MnO_2 full batteries assembled with different COFs membranes. Both full batteries incorporating the TP-DPY membrane exhibit a smaller voltage gap between the charge and discharge plateaus, indicating reduced polarization and more efficient interfacial redox kinetics. At identical current densities, these TP-DPY-based full batteries also deliver higher specific capacities, confirming that the rapid Zn^{2+} transport and partial desolvation facilitated by the TP-DPY membrane enhance intercalation kinetics. In addition, rate performance tests show that, with increasing current density, the capacity decay of TP-DPY-assembled full batteries is significantly less pronounced than that of TP-BPY-based and control batteries. When the current density is subsequently reduced, TP-BPY-assembled batteries nearly recover their original capacity, indicating that their capacity loss under high-rate conditions is primarily limited by kinetic constraints rather than irreversible structural degradation (Figure 5c-d). This performance can be attributed to the rapid Zn^{2+} transport and partial desolvation provided by the TP-DPY membrane, which facilitate efficient ion migration, minimize local concentration gradients, and maintain uniform intercalation throughout the cathode structure.

The cycling charge-discharge tests reveal that the full batteries with the GF separator experience an obvious short-circuit failure after fewer than 300 cycles (Figure 5e-f), which is consistent with previously reported performance for similar systems. The two full batteries assembled with the TP-BPY membrane did not experience short-

View Article Online
DOI: 10.1039/D6SC01290F

circuiting, yet their specific capacities showed significant decay after 1000 cycles, falling to less than 50% of the initial values. By comparison, the TP-DPY membrane enables the two full batteries to maintain highly stable specific capacities over 1000 cycles, retaining more than 85% of their initial values, while the Coulombic efficiency remains consistently around 100% with negligible fluctuations. We also characterized the cathode materials after the cycling test. Under the same tested conditions, SEM, EDS, and XRD analyses show that both cathodes maintain their structural integrity (Figure S29-30). The separator has minimal impact on their morphology and crystal structure. These results indicate that the enhancement of cycle stability observed in full batteries primarily arises from the effects of the COF membranes on the Zn anode and the electrolyte. The post-cycling analysis of the separator after long-term cycling revealed that it maintained uniform thickness and porosity (Figure S31-33) as well as chemical structural integrity (Figure S34), indicating excellent structural stability during operation.

Moreover, we evaluated the self-discharge behavior of full batteries assembled with two pyridinyl COF membranes, which is closely related to the spontaneous dissolution of the zinc anode in aqueous electrolytes. The self-discharge test was conducted by first fully charging the batteries to a specified capacity, followed by a 48-hour resting period under open-circuit conditions, and then discharging them to measure the remaining capacity (Figure 5g). The results exhibit that the full battery with the TP-DPY membrane retains more than 90% of its capacity (Figure 5g, Figure S35), significantly higher than those with the TP-BPY and GF separators,

View Article Online
DOI: 10.1039/D6SC01290F

demonstrating the excellent self-discharge suppression capability of TP-DPY. This is mainly attributed to the partial desolvation of Zn^{2+} induced by COFs membranes, which significantly suppresses self-discharge through both kinetic and thermodynamic mechanisms. Partially desolvated Zn^{2+} carries fewer water molecules, reducing the concentration of reactive hydrated ions at the zinc surface and accelerating ion diffusion away from the electrode, thereby lowering local overpotentials and mitigating spontaneous dissolution. Thermodynamically, the COFs-mediated coordination environment stabilizes the desolvated Zn^{2+} and increases the energy barrier for electron transfer and zinc oxidation, thus decreasing the driving force for self-discharge under open-circuit conditions.

Conclusion

In summary, this work has demonstrated that mono-pyridinyl-functionalized COF membranes exhibit rapid transport of hydrated ions while promoting their partial desolvation. By a combination of theoretical calculations and spectroscopic characterization, we have confirmed that this unique ion transport behavior originates from a soft Lewis acid-induced competitive coordination mechanism within the nanochannels of pyridinyl COFs membranes. This membrane-mediated rapid transport of desolvated hydrated ions can significantly enhance the reversibility and cycling stability of aqueous electrochemical energy storage devices. We performed a systematic proof-of-concept evaluation of the electrochemical performance of pyridinyl COFs membranes using aqueous zinc-ion batteries as a model system. Electrochemical

View Article Online
DOI: 10.1039/D6SC01290F

measurements indicate that this combination of rapid ion conduction and efficient desolvation enhances interfacial Zn^{2+} diffusion, lowers nucleation overpotentials, and regulates surface deposition kinetics, thereby promoting uniform zinc growth and effectively suppressing dendrite formation. Zinc metal electrodes paired with mono-pyridine COF membrane could maintain stable stripping/plating over 2000 cycles in a 2 M $ZnSO_4$ electrolyte without any additives, far exceeding the performance of currently employed aqueous battery separators. Full batteries tests using MnO_2 and V_2O_5 cathodes demonstrate that the mono-pyridine COFs membrane enables the batteries to retain more than 85% of their initial capacity after 1000 charge-discharge cycles. These results highlight the potential of COFs membranes as a platform for precise regulation of ion solvation and transport, offering a versatile strategy to enhance the efficiency, stability, and safety of next-generation aqueous electrochemical energy storage devices.

View Article Online
DOI: 10.1039/D6SC01290F

Acknowledgements

The authors acknowledge the finical support by the National Natural Science Foundation of China (Grant No. 52503041), and the Sichuan Provincial Department of Science and Technology (Grant No. 2025YFHZ0186), the Fundamental Research Funds for the Central Universities of China (Grant No. 20822041H4076), the Starting Grant from the Ministry of Education of China (Grant No. 0082204153346), and the financial support by the State Key Laboratory of Advanced Polymer Materials (Grant No. sklpme2024-2-16, sklpme2024-2-20).

Author contributions

S. Zhou proposed and supervised the project, conceptualized and designed the study, analyzed the data, and wrote the initial manuscript together with X. Li. X. Li carried out most of the experiments and theoretical calculations. J. Liu, Y. Zhang, Z. Dai, Z. Tan were responsible for material characterization. All authors participated in discussing the results and preparing the final manuscript.

Conflict of Interests

The authors declare no competing interests.

Supporting Information

Supplementary results are available online.

View Article Online
DOI: 10.1039/D6SC01290F

References

1. Joos, M.; Kang, X.; Merkle, R.; Maier, J., Water uptake of solids and its impact on ion transport. *Nature Materials* **2025**, 1-14.

2. Wei, Z.; Wang, Y.; Hong, H.; Chen, Z.; Chen, A.; Wang, S.; Yang, S.; Hou, Y.; Huang, Z.; Liang, G., Long-life aqueous zinc-iodine flow batteries enabled by selectively intercepting hydrated ions. *Nature Communications* **2025,** *16* (1), 9301.

3. Wang, A.; Breakwell, C.; Foglia, F.; Tan, R.; Lovell, L.; Wei, X.; Wong, T.; Meng, N.; Li, H.; Seel, A., Selective ion transport through hydrated micropores in polymer membranes. *Nature* **2024,** *635* (8038), 353-358.

4. Wang, G.; Shao, L.; Zhang, S., Membrane-Ion Interactions Creating Dual-Nanoconfined Channels for Superior Mixed Ion Separations. *Advanced Materials* **2025**, 2414898.

5. Yuan, Y.; Li, J.; Zhu, Y.; Qiao, Y.; Kang, Z.; Wang, Z.; Tian, X.; Huang, H.; Lai, W., Water in electrocatalysis. *Angewandte Chemie International Edition* **2025,** *64* (18), e202425590.

6. Liu, C.; Yang, Y.; Hong, W.; Ma, J. A.; Zhu, Y., Ion Hydration Enables Generality in Asymmetric Catalysis: Desymmetrization to P-Stereogenic Triarylphosphine Derivatives. *Angewandte Chemie* **2025,** *137* (6), e202417827.

7. Ye, B.; Wu, F.; Zhao, R.; Zhu, H.; Lv, M.; Han, X.; Chen, T.; Wang, X.; Bai, Y.; Wu, C., Electrolyte Regulation toward Cathodes with Enhanced-Performance in Aqueous Zinc Ion Batteries. *Advanced Materials* **2025,** *37* (15), 2501538.

8. Kondo, Y.; Abe, T.; Yamada, Y., Kinetics of interfacial ion transfer in lithium-ion batteries: Mechanism understanding and improvement strategies. *ACS applied materials & interfaces* **2022,** *14* (20), 22706-22718.

9. Zuo, P.; Ye, C.; Jiao, Z.; Luo, J.; Fang, J.; Schubert, U. S.; McKeown, N. B.; Liu, T. L.; Yang, Z.; Xu, T., Near-frictionless ion transport within triazine framework membranes. *Nature* **2023,** *617* (7960), 299-305.

10. Xu, R.; Yu, H.; Ren, J.; Zhang, W.; Kang, Y.; Wang, Z.; Feng, F.;

Xia, X.; Liu, J. Z.; Peng, L., Regulate ion transport in subnanochannel membranes by ion-pairing. *Journal of the American Chemical Society* **2025,** *147* (20), 17144-17151.

11. Lu, D.; Huang, M.; Zhang, C.; Bu, G.; Li, G.; Geng, Y.; Xu, S.; Xiang, X.; Qian, Y.; Lu, J., Impact of charge homogeneity on ion selectivity in polyamide membranes. *Nature Water* **2025**, 1-14.

12. Yang, H.; Chen, D.; Zhao, R.; Li, G.; Xu, H.; Li, L.; Liu, X.; Li, G.; Chao, D.; Han, W., Reunderstanding aqueous Zn electrochemistry from interfacial specific adsorption of solvation structures. *Energy & Environmental Science* **2023,** *16* (7), 2910-2923.

13. Zhang, J.; Liu, T.; Dong, X.; Chen, Z.; Tang, B.; Bu, F.; Li, H.-P.; Zhou, Z.; Chao, D.; Zhao, R., Electrolyte Coordination Environments in Wide-Temperature Aqueous Metal Batteries: Mechanisms and Design Strategies. *Chemical Science* **2026**.

14. Yang, F.; Yuwono, J. A.; Hao, J.; Long, J.; Yuan, L.; Wang, Y.; Liu, S.; Fan, Y.; Zhao, S.; Davey, K., Understanding H2 evolution electrochemistry to minimize solvated water impact on Zinc-anode performance. *Advanced Materials* **2022,** *34* (45), 2206754.

15. Wang, Y.; Wang, Z.; Pang, W. K.; Lie, W.; Yuwono, J. A.; Liang, G.; Liu, S.; Angelo, A. M. D.; Deng, J.; Fan, Y., Solvent control of water O− H bonds for highly reversible zinc ion batteries. *Nature Communications* **2023,** *14* (1), 2720.

16. Zhou, C.; Zhang, Z.; Zhang, M.; Sun, X.; Zhang, J.; Huang, G.; Na, Z., Targeted deflection of Zn^{2+} migration trajectory using the piezomagnetic effect to enable horizontal Zn deposition. *Energy & Environmental Science* **2025,** *18* (8), 3817-3827.

17. Bayaguud, A.; Fu, Y.; Zhu, C., Interfacial parasitic reactions of zinc anodes in zinc ion batteries: Underestimated corrosion and hydrogen evolution reactions and their suppression strategies. *Journal of Energy Chemistry* **2022,** *64*, 246-262.

18. Xu, T.; Wu, B.; Hou, L.; Zhu, Y.; Sheng, F.; Zhao, Z.; Dong, Y.; Liu, J.; Ye, B.; Li, X., Highly ion-permselective porous organic cage membranes with

hierarchical channels. *Journal of the American Chemical Society* **2022,** *144* (23), 10220-10229.

19. Li, Y.; Wang, Y.; Chen, B.; Lin, Y.; Zhang, G.; Avdeev, M.; Shi, S., Proactive Lithium Dendrite Regulation Enabled by Manipulating Separator Microstructure Using High-Fidelity Phase-Field Simulation. *Advanced Energy Materials* **2025**, 2500503.

20. Mi, Z.; Zhou, T.; Weng, W.; Unruangsri, J.; Hu, K.; Yang, W.; Wang, C.; Zhang, K. A.; Guo, J., Covalent organic frameworks enabling site isolation of viologen-derived electron-transfer mediators for stable photocatalytic hydrogen evolution. *Angewandte Chemie International Edition* **2021,** *60* (17), 9642-9649.

21. Liao, Q.; Li, Z.; Sun, Q.; Xu, H.; Wang, Y.; Xu, Y.; Wu, H.; Zhang, Z.; Xie, Y.; Li, H., Pyridine Functionalized β-Ketoenamine-Linked Covalent Organic Framework Nanostructures for H_2O_2 Photosynthesis. *ACS Applied Nano Materials* **2025,** *8* (16), 8095-8105.

22. Li, X.; Chen, F.; Ye, Y.; Wang, C.; Ding, G.; Zhang, Y.; Xiao, X.; Li, L.; Guo, Z. G.; Jia, L. C., A Mesoporous Ferroelectric Separator for Inner Helmholtz Plane Homogenization Enabling Zinc Anode with High Reversibility. *Small* **2025**, 2501855.

23. Chen, C.; Joshi, T.; Li, H.; Chavez, A. D.; Pedramrazi, Z.; Liu, P.-N.; Li, H.; Dichtel, W. R.; Bredas, J.-L.; Crommie, M. F., Local electronic structure of a single-layer porphyrin-containing covalent organic framework. *ACS nano* **2018,** *12* (1), 385-391.

24. Sun, R.; Yang, X.; Hu, X.; Guo, Y.; Zhang, Y.; Shu, C.; Yang, X.; Gao, H.; Wang, X.; Hussain, I., Unprecedented photocatalytic hydrogen peroxide production via covalent triazine frameworks constructed from fused building blocks. *Angewandte Chemie* **2025,** *137* (4), e202416350.

25. Yang, X.; An, Q.; Li, X.; Fu, Y.; Yang, S.; Liu, M.; Xu, Q.; Zeng, G., Charging modulation of the pyridine nitrogen of covalent organic frameworks for promoting oxygen reduction reaction. *Nature Communications* **2024,** *15* (1), 1889.

26. Luo, R.; Luo, X.; Xu, H.; Wan, S.; Lv, H.; Zou, B.; Wang, Y.; Liu, T.; Wu, C.; Chen, Q., Reticular ratchets for directing electrochemiluminescence. *Journal of the American Chemical Society* **2024,** *146* (24), 16681-16688.

27. Li, S.; Zhong, Y.; Huang, J.; Lai, G.; Li, L.; Jiang, L.; Xu, X.; Lu, B.; Liu, Y.; Zhou, J., Regulating interfacial kinetics boosts the durable A h-level zinc-ion batteries. *Energy & Environmental Science* **2025,** *18* (5), 2599-2609.

28. Li, Z.; Wang, Z.; Sun, W.; Ma, Y.; Guo, W.; Fu, Y., Regulating Interface Engineering by Helmholtz Plane Reconstructed Achieves Highly Reversible Zinc Metal Anodes. *Advanced Materials* **2025,** *37* (14), 2420489.

29. Wang, D.; Li, R.; Dong, J.; Bai, Z.; Wang, N.; Dou, S. X.; Yang, J., Bidentate Coordination Enables Anions-Regulated Solvation Structure for Advanced Aqueous Zinc Metal Batteries. *Angewandte Chemie International Edition* **2025,** *64* (2), e202414117.

30. Boyle, D. T.; Kong, X.; Pei, A.; Rudnicki, P. E.; Shi, F.; Huang, W.; Bao, Z.; Qin, J.; Cui, Y., Transient voltammetry with ultramicroelectrodes reveals the electron transfer kinetics of lithium metal anodes. *ACS Energy Letters* **2020,** *5* (3), 701-709.

31. Yang, H.; Fang, K.; Duan, J.; Dong, J.; Li, Y.; Yang, S.; Liang, J.; Jiang, Y.; Li, M.; Liu, Y., Selective facet shielding induced epitaxial deposition along the Zn (101) plane for highly reversible Zn-Ion batteries. *Energy Storage Materials* **2025,** *75*, 103995.

32. Liu, Z.; Zhang, X.; Liu, Z.; Jiang, Y.; Wu, D.; Huang, Y.; Hu, Z., Rescuing zinc anode–electrolyte interface: mechanisms, theoretical simulations and in situ characterizations. *Chemical Science* **2024,** *15* (19), 7010-7033.

33. Huang, Y.; Zhuang, Y.; Guo, L.; Lei, C.; Jiang, Y.; Liu, Z.; Zhao, Y.; Xing, K.; Wu, X.; Luo, S., Stabilizing anode-electrolyte interface for dendrite-free Zn -ion batteries through orientational plating with zinc aspartate additive. *Small* **2024,** *20* (10), 2306211.

34. Liu, X.; Wang, G.; Lv, Z.; Du, A.; Dong, S.; Cui, G., A perspective on uniform plating behavior of Mg metal anode: diffusion limited theory versus nucleation theory. *Advanced Materials* **2024,** *36* (9), 2306395.

35. Jin, S.; Yin, J.; Gao, X.; Sharma, A.; Chen, P.; Hong, S.; Zhao, Q.; Zheng, J.; Deng, Y.; Joo, Y. L., Production of fast-charge Zn-based aqueous batteries via interfacial adsorption of ion-oligomer complexes. *Nature communications* **2022,** *13* (1), 2283.

36. Kim, M.; Lee, J.; Kim, Y.; Park, Y.; Kim, H.; Choi, J. W., Surface overpotential as a key metric for the discharge–charge reversibility of aqueous zinc-ion batteries. *Journal of the American Chemical Society* **2023,** *145* (29), 15776-15787.

37. Cui, S.; Zhang, D.; Gan, Y., Traditional Electrochemical Zn^{2+} Intercalation/Extraction Mechanism Revisited: Unveiling Ion-Exchange Mediated Irreversible Zn^{2+} Intercalation for the δ-MnO_2 Cathode in Aqueous Zn Ion Batteries. *Advanced Energy Materials* **2024,** *14* (7), 2302655.

The data supporting this article have been included as part of the ESI

View Article Online
DOI: 10.1039/D6SC01290F